Scanning Microscopy

Volume 7 | Number 3 Article 9

9-3-1993

A Simulation Model for Electron Irradiation Induced Specimen Charging in a Scanning Electron Microscope

D. S. H. Chan
National University of Singapore

K. S. Sim
National University of Singapore

J. C. H. Phang
National University of Singapore

Follow this and additional works at: https://digitalcommons.usu.edu/microscopy

Part of the Biology Commons

Recommended Citation

Chan, D. S. H.; Sim, K. S.; and Phang, J. C. H. (1993) "A Simulation Model for Electron Irradiation Induced Specimen Charging in a Scanning Electron Microscope," *Scanning Microscopy*: Vol. 7 : No. 3 , Article 9.
Available at: https://digitalcommons.usu.edu/microscopy/vol7/iss3/9

This Article is brought to you for free and open access by the Western Dairy Center at DigitalCommons@USU. It has been accepted for inclusion in Scanning Microscopy by an authorized administrator of DigitalCommons@USU. For more information, please contact digitalcommons@usu.edu.

Scanning Microscopy, Vol. 7, No. 3, 1993 (Pages 847-859) 0891-7035/93$5.00+.00
Scanning Microscopy International, Chicago (AMF O'Hare), IL 60666 USA

A SIMULATION MODEL FOR ELECTRON IRRADIATION INDUCED SPECIMEN CHARGING IN A SCANNING ELECTRON MICROSCOPE

DSH Chan*, KS Sim and JCH Phang
Center for IC Failure Analysis and Reliability
Faculty of Engineering, National University of Singapore,
10 Kent Ridge Crescent, Singapore 0511

(Received for publication March 5, 1993, and in revised form September 3, 1993)

Abstract

A numerical model has been formulated to simulate the dynamics of specimen charging in a scanning electron microscope. In this model, the electric field due to imposed boundary conditions and fixed charges is solved by the finite element method. The empirical electron yield data are stored in "Universal Yield Curves (UYC)". These UYCs control the generation of secondary and backscattered electrons from various materials. The electrons emitted from electron-solid interactions are tracked using a leapfrog integration scheme. Excess charges generated on the surface of electrically floating solids are assigned to numerical grids using a linear charge redistribution scheme. The validity of the simulation model was verified by measurements in a special setup which consisted of several isolated electrodes in the SEM chamber. Excess currents generated inside each electrode due to electron irradiation were measured simultaneously. Measurements and simulation results are in broad agreement and show that electrically floating electrodes, not directly irradiated by the primary beam, can charge-up if they are irradiated by secondary electrons and backscattered electrons emitted from a nearby electrode. The polarity of charge generation on the electrically floating solid depends on its own material property, and also strongly on the potential distribution in the space surrounding the floating electrode.

Key Words: Scanning electron microscope, electron-beam testing, electron-solid interaction, specimen charging, simulation, finite element, trajectory tracking.

*Address for correspondence:
DSH Chan,
Centre for IC Failure Analysis & Reliability,
Faculty of Engineering,
National University of Singapore, 10 Kent Ridge Crescent,
Singapore 0511
Phone No: (65) 772-2117
Fax No: (65) 779-1103

Introduction

In the scanning electron microscope, electric fields can be generated inside and outside the charged specimen. A weak external field can cause several observable effects. These include deflection of the low energy secondary electrons, the presence of bright areas due to the increased emission of electrons as a result of repulsion by the negatively-charged specimen surface and dark areas due to the attraction of secondary electrons by the positive surface charges. Strong external fields can also deflect the primary beam and distort the raster scan image (Le Gressus et al., 1984), (Ichinokawa et al., 84), (Shaffner and Hearle, 1976). Specimen charging can introduce significant errors in quantitative work such as critical dimension measurements (Brunner and Schmid, 1986), voltage measurements (Nye and Dinnis, 1985) and electron-beam lithography (Cummings and Kiersh, 1989), (Itoh and Nakamura, 1989). On the positive side, specimen charging can be used for testing printed circuit boards (Brunner et al., 1988) and very large scale integrated package substrates (Lee et al., 1991).

In certain microscopy applications, specimen charging can be eliminated by coating the specimens with a conductive layer. However, for other applications (such as voltage measurement and electron-beam lithography), this procedure is not permissible. In these situations, specimen charging can be minimized or even eliminated by various charge neutralization schemes (Crawford, 1980), (Le Gressus et al., 1984) or by operating the SEM under certain beam conditions (Werner and Warmoltz, 1884), (Sugiyama et al., 1986), (Joy, 1989), (Kodama and Uchikawa, 1992).

In view of the importance of these effects on many electron beam techniques, there is a need for an improved understanding of the specimen charging phenomenon. This paper presents a numerical model to simulate the dynamics of specimen charging and verification of the model by experimental measurements.

The Theory of Specimen Charging

In the scanning electron microscope (SEM), when primary electrons (PEs) impinge on the specimen, secondary electrons (SEs) and backscattered electrons (BEs) are emitted.

In this paper, this entire spectrum of emitted electrons will be collectively known as secondaries (2Es).

The 2Es can impinge on other parts of the specimen and emit another series of electrons which will be known as tertiaries (3Es). However, the scintillator-photomultiplier detector of the SEM is not able to distinguish between the 2Es and 3Es, hence the classification here is only for convenience of presentation. The 3Es can also subsequently generate other electrons, and the process continues.

Electron-solid interaction can be summarized as

$$I_{PE} = I_{2Es} + I_{sp}(1) \qquad (1)$$

where I_{PE} is the primary beam current, I_{2Es} is the emitted 2Es current (i.e. $I_{SE} + I_{BE}$) and I_{sp} is the specimen current.

The ratio of I_{2Es} to I_{PE} is called the emission yield ($Y_{2Es} = I_{2Es} / I_{PE}$). For most materials, there are two energies called crossover points at which the yield is unity, i.e. the generated 2E current equals the impinging PE current (Seiler, 1983). These two crossover energies are designated E_{P1} and E_{P2}, where $E_{P2} > E_{P1}$. Below E_{P1}, and above E_{P2} the electron yield is less than unity. Between E_{P1} and E_{P2}, the yield is greater than one.

When the yield is greater than one, the generated current (I_{2Es}) is greater than the primary current (I_{PE}) and the specimen is depleted of electrons. On the other hand, when the yield is less than one, the generated current (I_{2Es}) is less than the impinging current (I_{PE}), the specimen experiences a net gain of electrons. In both cases, excess charges (either positive or negative) are generated in the specimen.

If the specimen has a conductive path to either a charge reservoir or sink, the excess charges will be neutralized and the specimen will remain at its initial potential. However, if no conductive path exists, these excess charges will accumulate and cause the potential on the specimen to change. In such a situation, the electrically floating specimen is said to be charging. In this paper, the charging of the specimen due to direct PE irradiation is classified as direct charging.

In some situations, certain portions of the specimen may not be irradiated directly by the primary beam. However, the generated 2Es may still impinge on these parts of the specimen. If these parts are electrically floating, it is likely that they will gain or lose charges causing the specimen to charge up negatively or positively. The charging up of specimens by secondary or tertiary irradiation is known as indirect charging.

Fig. 1 depicts a practical situation of specimen charging in electron-beam probing of decapsulated integrated circuit packages. After the selective decapsulation process, the die is usually sitting at the bottom of the insulator cavity. During electron beam probing, the cavity wall is usually not irradiated by the PEs, nevertheless, it can charge-up due to irradiation by the SEs and BEs emitted from the die.

Fig. 2 shows the interactions of the various parameters that control the dynamics of specimen charging. When the primary beam impinges on the die, it releases 2Es and generates excess charges in the die. The voltages on various conductors (boundary conditions) set up an electrostatic field around and within the specimen. The emitted 2Es interacts with this electric field as they leave the die. Depending on the boundary conditions, the 2Es may experience an extraction force that pulls them away from the die or a retarding force that suppresses them. In either cases, some of the 2Es will be redistributed onto the cavity wall. These 2Es interact with the insulating material, releasing 3Es and generating excess charges that charge-up the cavity wall as well.

The trapped excess charges on the die and cavity wall modify the electric field outside the solid which in turn modifies the trajectories of subsequent electrons. This process continues until a global steady state condition is achieved. At steady state, the charges added to the floating specimen is balanced by charges that leave them (via electron emission, charge conduction and leakage). In practice, the charging of cavity wall will stabilize after a while, due to charge leakage and beam induced conduction.

Overview of Simulation Model

This highly interactive specimen charging process is broken up into cyclic sequential modules to facilitate simulation in a computer. The cyclic sequential simulation model in Fig. 3 involves four major computational steps, namely:

a) solving the electric field distribution imposed by the

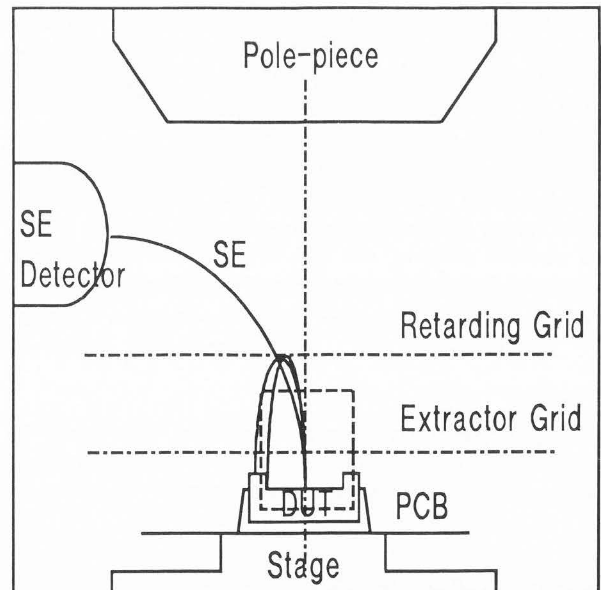

Fig. 1. Schematic diagram (not to scale) showing the measurement set-up for electron beam testing of integrated circuits in SEM. After the decapsulation process, the die is sitting in the insulator cavity. During probing, the cavity wall is not exposed to the primary electron, nevertheless, it can charge up due to bombardments by secondary electrons and backscattered electrons emitted from the die.

boundary conditions and the trapped and moving charges,
b) tracking electron trajectories (PE, 2Es, 3Es ..),
c) modeling electron-solid interaction leading to generation of 2Es and 3Es .., etc.
d) computing excess charge accumulation, conduction and redistribution on the specimens.

The electron irradiation induced conduction, charge leakage and voltage break-down in charged-up specimens are not modeled in this simulation. Subsequent sections describe the implementations of each computational step in greater detail.

Solution of Electric Field

The potential distribution of the physical system is fully described by the Poisson equation and the imposed boundary conditions. Two sets of first-order finite element (Silvester and Ferrari, 1983) routines were developed for electric potential calculation and field interpolation; a 2-dimensional cartesian co-ordinate finite element routine (2D-FEM) for all type of physical structures and an axisymmetry cylindrical coordinate finite element routine (AX-FEM) for rotational symmetry structures. In this work, the simulation domain is discretized into square and rectangular meshes (whenever possible) to facilitate tracking of electron trajectories. Note that only the electric potential and field calculation routines are different, all other computational steps (electron emissions, trajectory tracking and excess charges distribution) use a same set of routines regardless of the choice of the co-ordinate systems.

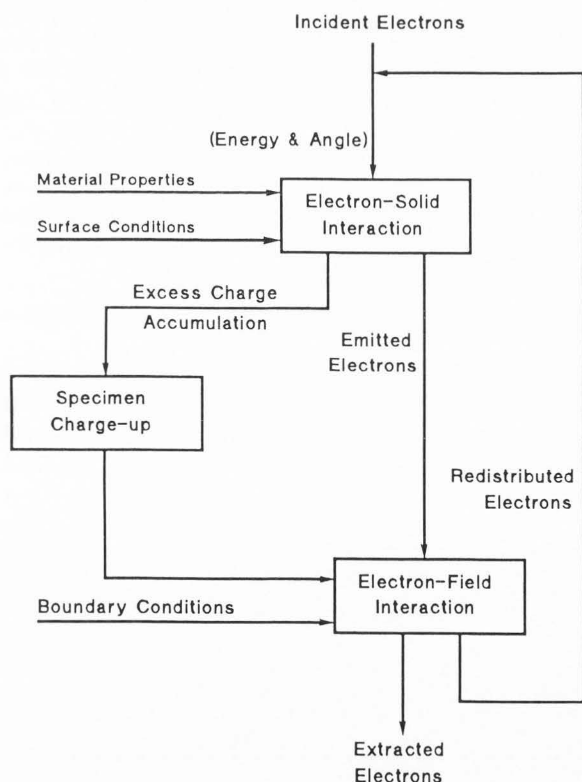

Fig. 2. A schematic diagram showing the interaction of various parameters that control the dynamics of specimen charging in the SEM.

Electron Solid Interaction

When an electron impinges on a solid, SEs and BEs are generated with specific energy and angular distributions. In this simulation model, the yield of SEs and BEs from various materials are represented by a set of "Universal Yield Curve".

Secondary Electron Emission

A universal SE yield curve relates the SE yield of a material at a given incidence energy and angle $\delta(E, \alpha)$ to the maximum yield δ_{MAX} and the corresponding energy E_{MAX}. There are many versions of universal yield curves in the literature. Most of these yield curves (Burke, 1980), (Salehi and Flinn, 1980), (Seiler, 1983) are derived for normal

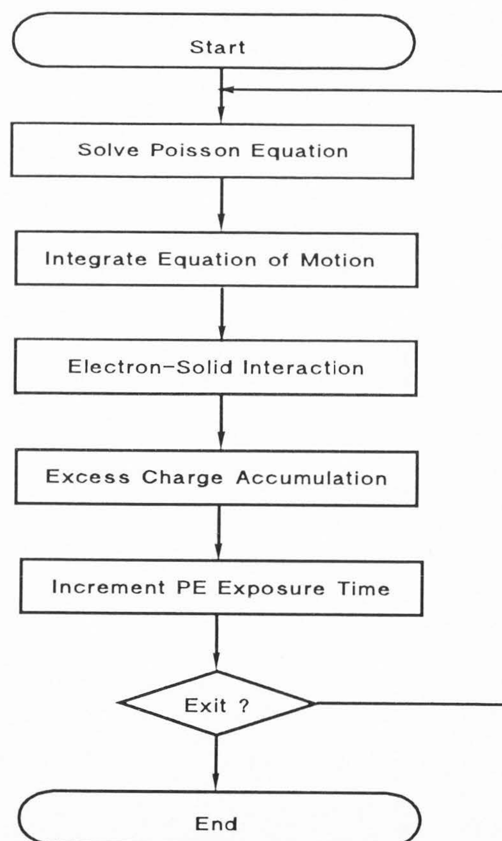

Fig. 3. Block diagram of electron beam induced specimen charging simulation model. This cyclic sequential simulation model consists of four main modules: Poisson solver module, electron-solid interaction module, particle trajectories tracking module and excess charge generation and handling module.

incidence. At oblique incidence, the SE yield is assumed to be inversely proportional to the cosine of the incidence angle (Seiler, 1983). This inverse cosine law, however, overestimates the oblique SE yield at low incidence energy.

Kodama (Kodama and Uchikawa, 1992) and Ishibashi (Ishibashi et al., 1992) extended Seiler's (Seiler, 1983) formulation to account for oblique incidence. However, this improved formulation still contained an inverse cosine term which becomes problematic when the incident angle is close to 90°. Bouchard (Bouchard and Carette, 1980) took both the oblique incidence and specimen surface roughness into consideration and derived an accurate SE yield curve for low energy range. However, Bouchard's SE yield curve is complicated and involves an integration term which must be evaluated numerically. As a result of this assessment, the SE yield curve proposed by Vaughan (Vaughan, 1989) is found to be the most suitable for this simulation. This SE yield curve which takes both the oblique incidence and specimen surface roughness into consideration, is reasonably accurate and can be evaluated easily.

In Vaughan's formulation, δ_{MAX} and E_{MAX} are corrected for oblique incidence. These corrected values are then used to calculate the SE yield. The empirical correction formulas for δ_{MAX} and E_{MAX} are:

$$E_{MAX}(\alpha) = E_{MAXO}\left(1 + K_S \frac{\alpha^2}{\pi}\right) \quad \text{for } 0 \le \alpha < \frac{\pi}{2}$$

$$\delta_{MAX}(\alpha) = \delta_{MAXO}\left(1 + K_S \frac{\alpha^2}{2\pi}\right) \quad \text{for } 0 \le \alpha < \frac{\pi}{2} \qquad (2)$$

where K_S, a "smoothness factor" of the surface, ranges from 0 for a textured surface to 1 for a dull surface and 1.5 or 2 for a polished crystalline surface. δ_{MAXO} and E_{MAXO} are the maximum SE yield and the corresponding energy at normal incidence. The SE yield curve is then given by:

$$\delta(E,\alpha) = \begin{cases} 1.113\,\delta_{MAX}(\alpha) * \left(\frac{E_{MAX}(\alpha)}{E}\right)^{0.35} & \text{for } E > 3E_{MAX}(\alpha) \\ \delta_{MAX}(\alpha)\left(V e^{(1-V)}\right)^{K} & \text{for } E \le 3E_{MAX}(\alpha) \end{cases} \qquad (3)$$

$$\text{Where } V = \frac{E - E_O}{E_{MAX}(\alpha) - E_O} \qquad (4)$$

$$K = \begin{cases} 0.62 & \text{for } V \le 1 \\ 0.25 & \text{for } V > 1 \end{cases} \qquad (5)$$

and E_O is the cut-off energy below which there is no SE emission.

Fig. 4 is a comparison of Vaughan's (Vaughan, 1989) and Seiler's (Seiler, 1983) universal yield curves at zero and 60° incidence. The measured data is reproduced from

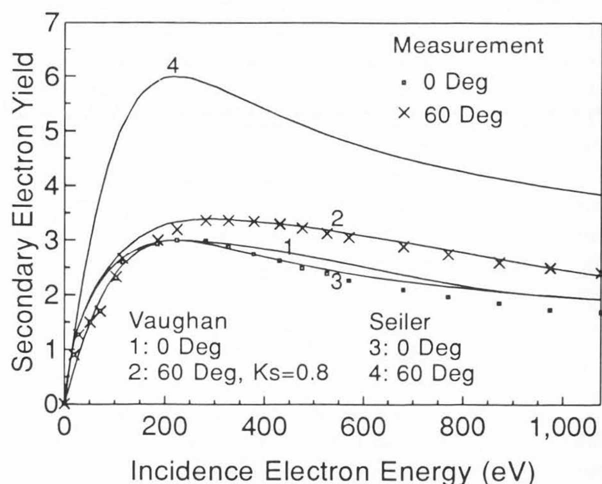

Fig. 4. A comparison of Seilier's (Seiler, 1983) and Vaughan's (Vaughan, 1989) SE yield curves at normal and 60° incidence. The measurement SE yield of reduced lead glass is reproduced from Bouchard (Bouchard and Corette, 1980).

Bouchard's work (Bouchard and Carette, 1980). At normal incidence, both sets of yield curves are very close to the measured data. At 60° incidence, Vaughan's yield curve (with K_S = 0.8) fits the measured data well, whereas, the inverse cosine law overestimates the oblique SE yield.

Secondary electrons (SE) are emitted from solid into vacuum with a specific energy distribution and each energy component is emitted with a Lambert cosine distribution. These energy and angular distributions are approximated by the following normalized equations in the 2-dimensional simulation model. For a metallic target, it is given by (Kollath, 1956):

$$N_{SE}(E', W, \theta) = \frac{W \times \exp(2 - \sqrt{2.667 \times W})}{\int_0^{E'} W \times \exp(2 - \sqrt{2.667 \times W})\, dW} \times \frac{\cos(\theta)}{2} \qquad (6)$$

For an insulating target it is given by (Seggern, 1985):

$$N_{SE}(E', W, \theta) = \frac{\exp(-0.4 \times W) - \exp(-2.5 \times W)}{\int_0^{E'} [\exp(-0.4 \times W) - \exp(-2.5 \times W)]dW} \times \frac{\cos(\theta)}{2} \qquad (7)$$

where E' = 50 eV if incident electron energy (E) > 50 or E' = E if E < 50 and θ is the emission angle measured from surface normal.

Fig. 5 shows that both types of targets have similar normalized SE spectrum. However, the insulator target has a sharper maximum, whereas the metallic target has broader full width half maximum (FWHM).

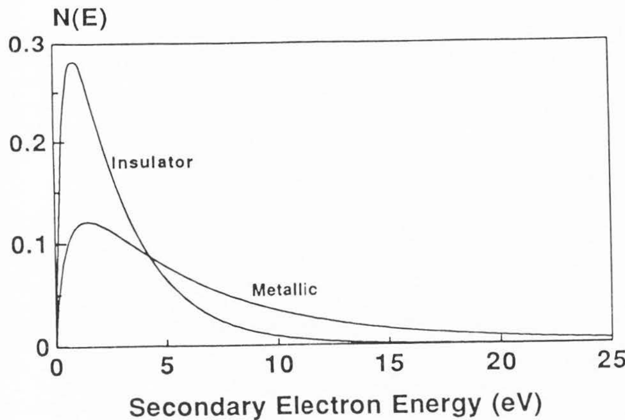

Fig. 5. Normalized secondary electron energy spectrum of metallic and insulating materials.

Backscattered Electron Emission

At high beam energies (> 40 keV), BE yield from a solid is independent of incoming electron energy. As beam energy decreases, the BE yield increases (Darlington and Cosslett, 1972) and then decreases again as beam energy approaches zero (Gibbons, 1966). There are no known equations for the BE yield at the low beam energy range. In this simulation, the BE yield is approximated by a set of piece-wise equations:

$$\eta(E,\alpha)=\begin{cases} K_0(E \times 10^{-3})^{-K_1} & \text{for } E > E_{BMAX} \\ \eta_o + E\left[\dfrac{\eta_{MAX} - \eta_o}{E_{BMAX}}\right] & \text{for } 0 \le E \le E_{BMAX} \end{cases} \quad (8)$$

where E_{BMAX} is electron incident energy at which η is maximum. η_{MAX} is the maximum value of η and η_0 is the value of η when electron incident energy (E) is zero.

K_0 and K_1 are constants which can be determined if (E_{BMAX}, η_{MAX}) and one set of (E, η(E)) are known. Generally, BE yield increases slightly with oblique incidence angle (α) up to 20°, and rapidly above 30°, with the yield tending toward unity at grazing incidence. In this simulation, the BE yield as a function of oblique incidence is approximated by a set of piece-wise equations given by:

$$\eta(E,\alpha)=\begin{cases} \eta_o(E) & \text{for } \alpha \le 30^\circ \\ \eta_o(E) + K_B\dfrac{\alpha - 30}{60}(1-\eta_o(E)) & \text{for } 30^\circ < \alpha \le 90^\circ \end{cases} \quad (9)$$

where K_B is the "surface smoothness factor". Its value ranges from 0 for a textured surface to 1 for a polished crystalline surface.

The energy and angular distribution of BEs are highly dependent on the properties of target material, electron incidence energy and incidence angle. Generally, when the incidence angle is less than 50°, electrons are backscattered with a cosine distribution. BE spectrums of high atomic number solids have a very sharp peak at energy just below the incident beam energy. As the atomic number of target decreases, the peak of BE spectrum broadens and shifts toward the low energy region.

When the beam incident angle is larger than 60°, the angular distribution of BE contains a pronounced forward lobe of electrons that have lost less than 10% of the incident energy. The BEs that do not lie in the forward lobe, have lost (on the average) 50% of the incident energy (Niedrig, 1982). Measurements by Wells (Wells, 1975) show that, at 60° incidence, the peak of BE spectrum shifts to the low energy region as the take off angle increases. Each spectral component has its own angular distribution; the high energy spectral components have more directed angular distribution (forward lobes), whereas the low energy BEs have more diffused angular distribution (cosine).

Many researchers have attempted to approximate the high oblique angle BE emission using combined diffusion and single scattering event models (Wells, 1974), (Niedrig, 1982). In all these models, the single scattering event was represented by the Rutherford cross-section. The approximation is invalid at low beam energy (< 10 keV). The analytical models for the energy and angular distributions of BE (Wells, 1974), (Niedrig, 1982) are not just inaccurate at low incident energy, but they are also complicated and difficult to apply. An approximate model is used in this simulation, with the following properties:

a. The BE spectrum is assumed to be independent of PE incident angle and is approximated by a triangular shape distribution function:

$$N_{BE}(W, E) = 2.0 \times W/E^2; \quad \text{for } E > 0 \qquad (10)$$
$$N_{BE}(0, 0) = 1.0; \quad \text{for } E = 0.0$$

where W is the energy of the emitted BE and E is the energy of incident electron. Equation (10) is normalized such that the area under the triangle is one.

b. The BE angular distribution is assumed to be independent of BE spectral components -each spectra component has the same cosine angular distribution.

Super-Particle Representation

The moving electrons are uncorrelated and their density is low so that the interactions among the moving particles can be ignored. In solving the Poisson equation, one can safely ignore the moving charge density. Since there are no interaction among the moving charges, all the PEs in any time interval T_{EX} can be represented by a super-particle of energy E_{PE} carrying a charge

$$Q_{PE} = I_{PE}\, T_{EX} \qquad (11)$$

where time interval T_{EX} is defined as the PE exposure time.

To save computational time and memory requirements, the energy spectrum is discretized into bands. All 2Es in a particular band are considered to have energy W_j, where W_j is the average energy of band j. Similarly, the angular distribution is also discretized into sectors; all 2Es falling in that particular sector k are represented by angle θ_k. In this way, each energy and angular combination is represented by one super-particle having initial energy W_j and emission angle θ_k. The charge carried by each super particle is

$$Q_n = \begin{cases} Q_{PE} \cdot \delta(E,\alpha)\, A_j^W\, A_k^\theta & \text{for } 0 < W \le 50 \text{ eV} \\ Q_{PE} \cdot \eta(E,\alpha)\, A_j^W\, A_k^\theta & \text{for } 50 < W < E \end{cases} \tag{12}$$

where A_j^W and A_k^θ are the area of the energy band j and the sector k respectively.

From the initial energy and emission angle, the x and y components of the super-particle velocity (V_x, V_y) are calculated. The electron emission point is taken to be at the impinging point. These initial conditions, i.e. position (x, y) and velocity (V_x, V_y), fully characterize the emitted 2Es. These initial conditions are then loaded into a set of arrays containing similar information for all other traveling super-particles.

Tracking Of Electron Trajectories

Once the emitted 2Es are grouped into super particles, their subsequent status (i.e. position and velocity) in the electric field are tracked by a leapfrog (Birdsall and Langdon, 1985) integration scheme. The kinetic energy of an electron in a quasi-static electric field is directly related to its velocity. As a result, a change in the electron velocity also results in a corresponding change in the kinetic energy of the electron. In this leapfrog integration scheme, the equation of motion for electrons in an electrostatic field is represented by two first order centre difference equations (see also Fig. 6):

$$\bar{v}_{(t+\frac{\Delta t}{2})} = \bar{v}_{(t-\frac{\Delta t}{2})} + \frac{q}{m}\bar{E}(\bar{r},t)\Delta t$$

$$\bar{r}_{(t+\Delta t)} = \bar{r}_t + \bar{v}_{(t+\frac{\Delta t}{2})}\Delta t \tag{13}$$

where q and m are the charge and the mass of an electron, $\bar{v}_t$ and $\bar{r}_t$ are the velocity and position vectors of the electron at time t, $\bar{E}(\bar{r},t)$ is the electric field vector at position $\bar{r}_t$ at time t, Δt is the trajectory integration time step.

This algorithm requires the calculation of electric field along the trajectory path. The potential anywhere within a particular mesh is given by:

$$\phi(x,y) = N_1\phi_1 + N_2\phi_2 + N_3\phi_3 + N_4\phi_4 \tag{14}$$

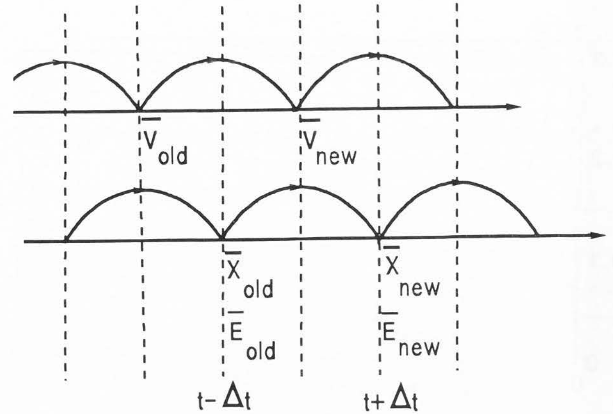

Fig. 6. Sketch of leapfrog integration method showing time centering of field while advancing velocity vector, and centering of velocity vector while advancing position vector.

where suffixes 1, 2, 3 and 4 are defined in an anti-clockwise direction as illustrated in Fig 7. N_1, N_2, N_3 and N_4, are the shape functions of that particular element which, assuming it is rectangular are:

$$N_1 = (1-\xi)(1-\zeta) \qquad N_2 = \xi(1-\zeta)$$
$$N_3 = \xi\zeta \qquad N_4 = (1-\xi)\zeta \tag{15}$$

$$\text{for} \quad \xi = \frac{x - x_1}{x_2 - x_1} \qquad \zeta = \frac{y - y_1}{y_2 - y_1} \tag{16}$$

The electrostatic field within this mesh is calculated by taking the negative gradient of Eqn (14).

A particle is tracked until it has traveled out of the simulation domain or has impinged on a solid. When a particle impinges on a solid, it generates subsequent spectra of SEs and BEs (3Es). These 3Es (after being grouped into super-particles) are loaded into the particle array and from then on is no different from any other particles.

Limiting the Particle Population

In order to limit the population growth of particles, the program checks the charge emitted by each particle after it impinges on a solid. No subsequent particles will be generated if the emitted charge ($Q_{emitted}$) is less than a certain percentage factor (R_C) of Q_{PE}:

$$Q_{emitted} = Q_{incidence}\big(\delta(E,\alpha) + \eta(E,\alpha)\big) \le R_C Q_{PE} \tag{17}$$

The particle array is scanned periodically and all the similar particles are combined into one. Two particles i and j are considered similar if and only if its phase vector satisfies the following condition:

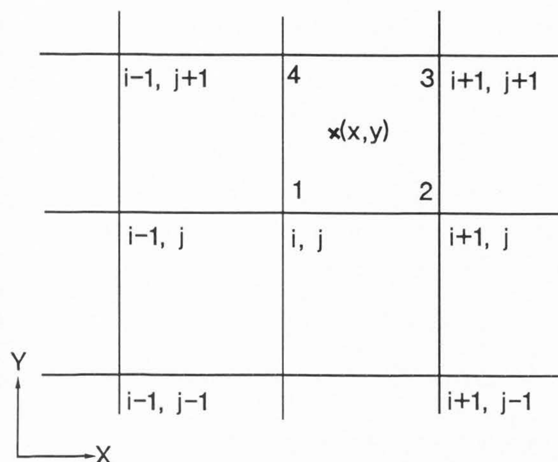

Fig. 7. Mesh indices and local nodes labeling for field interpolation.

$$\left(\left|X_i - X_j\right| \le \varepsilon_r\right) \cap \left(\left|Y_i - Y_j\right| \le \varepsilon_r\right) \cap \left(\left|Vx_i - Vx_j\right| \le \varepsilon_v\right) \cap \left(\left|Vy_i - Vy_j\right| \le \varepsilon_v\right) \tag{18}$$

The charge of the new particle is equal to the sum of all the charges of the similar particles, and the new phase vector is the mean of all the similar phase vectors. The percentage factor (R_C) and the tolerance factors (ε_r and ε_v) are specified by the user.

Treatment of Excess Charges in Insulators

The interaction of incidence electrons with solids and the subsequent emission of SEs and BEs produce excess charges in the solid. When excess charges are generated in the insulator, they remain at the point where they are generated, and as a result, a localized surface charge density is produced on the insulator surface. These charges are assigned to the nearest grid points using a charge redistribution scheme depicted in Fig. 8. When the excess charge of q is generated at point x between nodes x_1 and x_2, this charge is assigned to the grid nodes respectively:

$$q_1 = q(1 - \xi) \qquad q_2 = q\xi \tag{19}$$

where ξ is defined in equation (16). This global nodal charge density is updated at the end of each PE exposure time step T_{EX}. The new potential distribution of the entire system can then be computed from the Poisson equation. The excess charge density can have a significant effect on the trajectories of traveling super particles, and thus the PE exposure step T_{EX} must not be too long.

Localized nodal charge density produces field gradients within the insulator itself and also between the insulator and the nearby conductors. When the field gradient within the insulator surface reaches a certain critical value, conduction

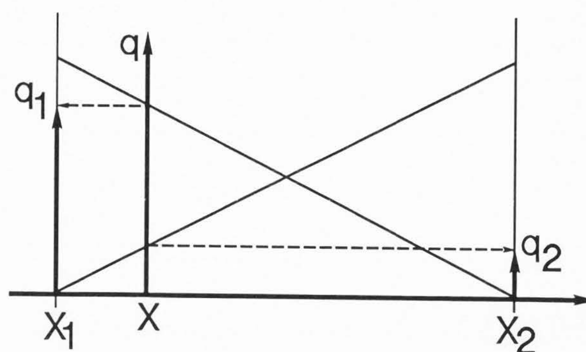

Fig. 8. The linear charge assignment scheme. A point charge generated between two nodes is redistributed linearly to the two nodes.

processes can take place and the local charge density gradient is reduced. Similarly, when the field gradient between the insulator surface and the nearby conductor exceeds the breakdown threshold of the vacuum, discharge takes place which reduces the charge density on the insulator surface. These discharge processes, however, are not included in this model.

Experimental Verification of Simulation Model

In practice, it is difficult to measure the charge distribution on a specimen inside the SEM chamber. In order to verify the validity of the simulation model, an experiment is devised involving the setup shown in Fig. 9. This setup consists of a special structure that resembles the region enclosed in the dotted box in Fig 1. The IC package material is now replaced by an aluminum ring. The IC die is replaced by an aluminum target with a built-in Faraday Cup. A shield plate is added above the extraction plate to minimize the influence of extraction potential on the primary beam trajectory. The extraction plate, the ring, the target and the shield plate are respectively connected to channel SMU1, SMU2, SMU3 and SMU4 of a HP4145B semiconductor parameter analyzer. Channel SMU4 is also connected to the SEM chamber ground and serves as a reference. PA1, PA2 and PA3 are the internal pico ammeters of the parameter analyzer.

When the PE is aimed into the Faraday cup, PA3 measures the primary beam current. When PE is impinging on the target surface, PA1, PA2 and PA3 measures the current due to the excess charges generated inside the extraction plate, the target and the ring respectively. The readings of PA1, PA2 and PA3 are recorded while the extraction plate voltage is increased slowly from -100V to +100V in steps of 5V.

The parameters used in this simulation are summarized in Table I. The yield data of the aluminum electrodes are measured in the SEM (Vacuum = 10^{-6} hectoPascal). These values are higher than the values reported in the literature

Table I. Summary of parameters used to verify the validity of the simulation model.

a) Primary Beam : Energy = 1 keV Current = 1 nA

b) Electron Yield of Aluminum Target (polished and sputtered with gold)

SE Yield :	δ_{MAX} = 1.576	E_{MAX} = 300 eV
	K_S = 1.0	E_O = 12.0 eV
BE Yield :	η_{MAX} = 0.430	E_{BMAX} = 12.0 eV
	K_o = 0.275	K_1 = 0.101
	η_o = 0.0	K_B = 0.7

c) Electron Yield of Aluminium Ring and Extraction Plate (polished)

SE Yield :	δ_{MAX} = 2.16	E_{MAX} = 300 eV
	K_S = 0.5	E_O = 12.0 eV
BE Yield :	η_{MAX} = 0.5	E_{BMAX} = 12.0 eV
	K_o = 0.275	K_1 = 0.101
	η_o = 0.0	K_B = 0.5

d) Discretized Energy and Angular Distribution

SE Spectrum:	17 Bands (nonlinear)
BE Spectrum:	4 Bands (nonlinear)
Angular Distribution:	18 Sectors (linear, 10° each)

f) Basic time step Δt: 500 fs.

e) PE Exposure time T_{EX}: 1.0 second

g) Percentage factor R_c: 10^{-4}

h) Tolerance factors: $\varepsilon_r = 0.1\ \mu m$, $\varepsilon_v = 1$ eV

because the specimen was not a pure aluminum sample and the measurement environment was not in ultra high vacuum.

Discussions

Fig. 10 shows that the simulation results and the measurement results are in good agreement over the entire range of extraction voltage. Iex, Isp and Irg are the extraction plate, target and ring current respectively normalized with respect to beam current. Isum is the sum of Isp, Irg and Iex. Solid lines are measurement results. Dotted lines are results of simulation using an axisymmetry cylindrical coordinate system, and the dashed lines are results of simulation using a 2-dimensional cartesian coordinate system. Note that the beam current is an electron current. Hence a negative normalized Isp means that excess positive charges are being generated in the target and are flowing out to the electrical ground. On the other hand, a positive normalized Isp means that excess electrons are being generated inside the target and are flowing out to the electrical ground. This polarity convention is also used for the normalized ring current Irg and normalized extractor current Iex.

The total emission yield of the aluminium target at 1 keV beam energy is greater than unity, thus positive excess charges are generated inside the target by the incident beam. The electric field produced by the entire range of extraction voltage is not strong enough to significantly affect the

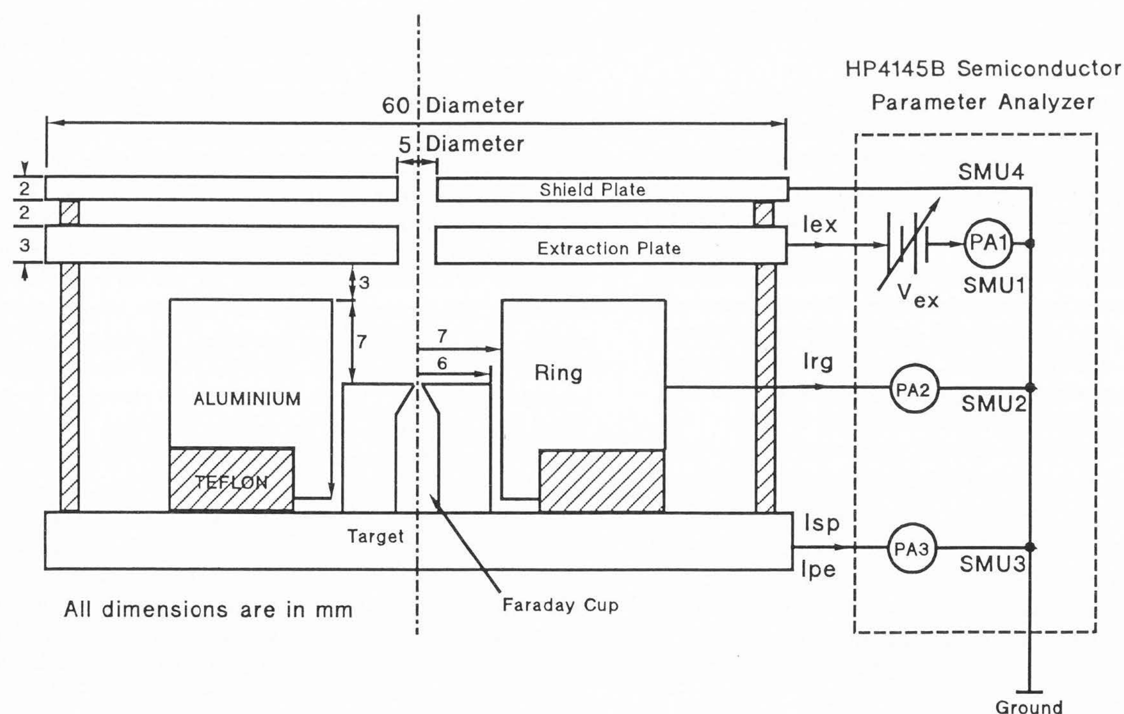

Fig. 9. Measurement setup for verifying the validity of the simulation model. SMU1, SMU2, SMU3 and SMU4 are four channels of the semiconductor parameter analyzer. PA1, PA2 and PA3 are internal pico ammeters of the parameter analyzer. They are used to measure the excess charges generated in the electrodes. All the electrodes are machined from aluminum alloy.

trajectories of BEs emitted from the target. As a result, the BEs emitted from the target with emission angles less than 45° (approximate) are intercepted by the extraction plate, whereas, the BEs with emission angle larger than 45° are intercepted by the ring. These energetic BEs also generate excess positive charges inside the ring and the extraction plate.

When a high positive voltage is applied to the extraction plate, it attracts and absorbs almost all the SEs emitted from the target, the ring and the extraction plate itself. The amount of SEs absorbed by the extraction plate is much larger than the positive excess charges generated by the BEs from the target; hence, a large electron current flows out of the extraction plate. Since no SE falls on the target and the ring, the positive current inside both of them (Isp and Irg) are constant for extraction voltage greater than 25V.

At a lower positive extraction voltage, SEs (from the target) with large emission angle are also intercepted by the ring. The excess electrons generated by these low energy incident electrons (with a yield much less than unity) compensate for the positive charges generated by the energetic BEs. When the extraction voltage is around -5V, almost all the SEs (from the target and the extraction plate) are collected by the ring. As the extraction voltage becomes more negative, more SEs (from the target, ring and the extraction plate) are repelled toward the target. As a result, the negative current in the target increases, whereas, the negative current in the ring decreases. At negative extraction voltages, the constant positive Iex is due to BEs from the target.

Fig. 10 shows that simulation error only occurs when the current in an electrode is negative (positive I/I_{PE}). This corresponds to the interaction of SEs with the electrode. At negative extraction voltages, the negative error in Isp

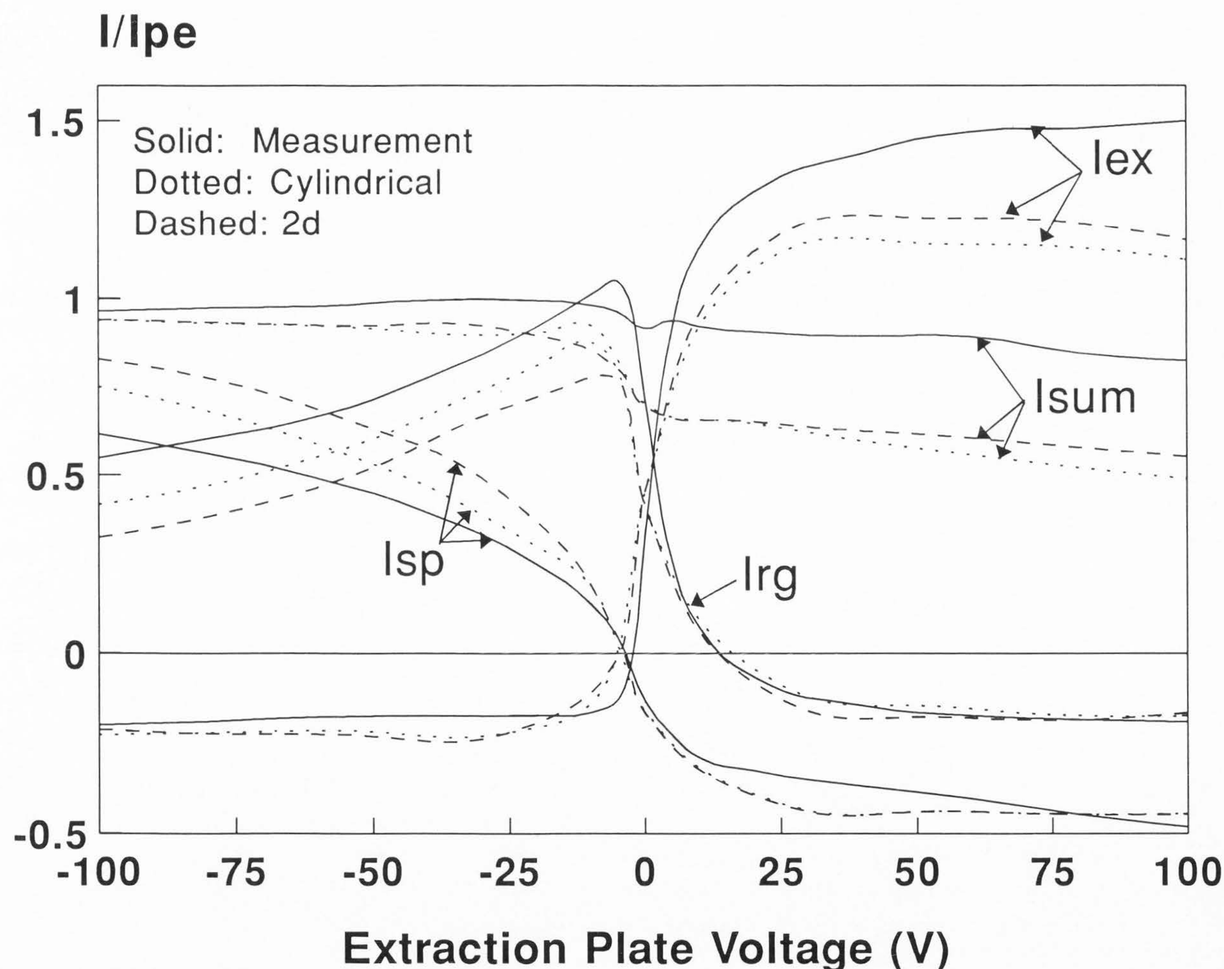

Fig. 10. Comparison of simulation and measurement results obtained from the special structure. Isp, Iex and Irg are the target, extraction plate and ring current respectively normalized with respect to beam current. Isum is the sum of Iex, Irg and Isp. Solid lines represent the measured data, whereas the dotted lines and dashed lines are simulated data. Dotted Lines are simulation results obtained using an axisymmetry cylindrical coordinate system. Dashed lines are results from a 2-dimensional simulation.

compensates the positive error in Irg, thus the simulated Isum is very close to the measured Isum. At positive extraction voltages, simulation error occurs only in Iex. These errors are mainly due to errors in electric field estimation and trajectory tracking of SEs. At each leapfrog integration step, any error in the calculated electric field will cause the electron to deviate from its actual path. This trajectory error is cumulative and becomes significant after many integration steps.

The 2-dimensional finite element (2D-FEM) solution of potential in the cylindrical cavity over-estimates the actual potential distribution near the target surface by about 200%. Hence, for any given extraction grid voltage, the calculated electric field just above the target surface is always much stronger than the actual field. At negative extraction voltages, a higher calculated retarding field suppresses more SEs back to the target. Consequently, the simulated Isp is higher than the measured Isp and the simulated Irg is lower than the measured Irg. At positive extraction voltages, the focusing action of the calculated electric field is stronger, as a consequence, more SEs leave the structure through the hole (5mm diameter) on the extraction plate.

Scalar potential calculated from an axisymmetry cylindrical coordinate finite element system (AX-FEM) is only accurate for regions far away from the axis of rotational symmetry. Estimation error is higher at regions closer to the axis of symmetry. In fact, the estimation error is worst along the paraxial region (Kasper, 1982). Since the electric field estimated from the AX-FEM is more accurate at regions close to the ring and target surface, the errors in Irg and Isp are lower at negative extraction voltages. Along the paraxial region, the estimation error of the AX-FEM is slightly larger than that of the 2D-FEM. As a result, the error in Iex is also larger when using AX-FEM.

Overall, the simulation results of the axisymmetry system are more accurate than the 2-dimensional cartesian system. A true 3-dimensional FEM system with higher order elements (especially along the paraxial region) is needed to improve the accuracy of the simulation. More accurate field interpolation and trajectory integration schemes may improve the accuracy of simulation at the expense of computation time.

The selection of discretized energy and angular distribution represents a compromise between accuracy and computational time and memory requirement. With this selection (Table 1), when a PE super-particle impinges on the target, 378 2E super-particles are generated. After all the 378 2Es have impinged on the surrounding solids, there will be a total of 142884 (378 x 378) 3Es super-particles. The parameter R_C limits the exponential growth of the super-particles to a manageable size. Simulations have shown that finer discretization of energy and angular distribution and the selection of smaller R_C also improve the accuracy of the model.

Conclusions

In summary, a simulation model has been developed to study the dynamics of specimen charging in a SEM. The simulation results are in good agreement with measurements despite many assumptions and approximations needed to make the computation achievable in a realistic time. Measurements and simulation results have shown that electrically floating electrodes not directly irradiated by the primary beam can charge-up if they are irradiated by SEs and BEs emitted from nearby specimens. The polarity of charge generated on the electrically floating solid depends not just on its own material property, it is also strongly dependent on the potential distribution in the space surrounding the floating electrode.

Acknowledgments

The authors thank Dr. WK Chim of the Center for IC Failure Analysis and Reliability, National University of Singapore and Dr. VRM Rao of Intel Corporation, Santa Clara, USA for helpful discussions on this topic. We appreciate the assistance of Mr. LH Chan for fabricating the special structure. This work is supported under National University of Singapore Research Project No. 900614.

References

Birdsall CK, Langdon AB (1985). Plasma Physics Via Computer Simulation. McGraw-Hill Book Company, Singapore: chapter **3**.

Bouchard C, Carette JD (1980). The secondary electron emission coefficient of disordered surfaces. Surface Science **100**: 241-250.

Brunner M, Schmid R (1986). Charging effects in low-voltage scanning electron microscope metrology. Scanning Electron Microsc. 1986; **II**: 377 - 382.

Brunner M, Kolbenschlag N, Westerman G, Lischke B (1988). Bare-board testing: the charge storage problem. Microelectronics Engineering **8**: 25 - 35.

Burke EA (1980). Secondary emission from polymers. IEEE Trans. Nucl. Sci. **27**: 1760 - 1764.

Crawford CK (1980). Ion charge neutralization effects in scanning electron microscopy. Scanning Electron Microsc. 1980; **IV**: 11 - 24.

Cummings KD, Kiersh M (1989). Charging effects from electron beam lithography. J. Vac. Sci. Technol. (B) **7**: 1536 - 1539.

Darlington EH, Cosslett VE (1972). Backscattering of 0.5-10 keV electrons from solid targets. J. Phys. D.: Appl. Phys. **5**: 1969 - 1981.

Gibbons DJ (1966). Secondary electron emission. Handbook Of Vacuum Physics. Edited by Beck AH, Pergamon Press, Oxford; Vol **2(3)**: 299 - 395.

Ichinokawa T, Hyama M, Onoguchi A (1984). Charging effect of specimen in scanning electron microscope. Jap. J. Appl. Phys. **13**: 1272 - 1277.

Ishibashi Y, Kodama T, Oiwa H, Uchikawa Y (1992). Analysis of electron range versus energy relationship of insulators in low-voltage scanning electron microscopy. Scanning **14**: 219-223.

Itoh H, Nakamura K (1989). Investigation of the charging effects on the thin SiO_2 layers with the electron beam lithography system. J. Vac. Sci. Technol. (B) **7**: 1532 - 1535.

Joy DC (1989). Control of charging in low-voltage SEM. Scanning **11**: 1- 4.

Kasper E (1982). Magnetic field calculation and determination of electron trajectories. Topics In Current Physics: Magnetic Electron Lenses (edited by Hawkes PW) **18**: 57-117.

Kollath R (1956). Sekundarelektronen-emission fester Korper bei Bestrahlung mit Electronen (Secondary electron emission from solid matter by electron irradiation). Handbuch der Physik, Spinger, Berlin, **21**: 232 -303.

Kodama T, Uchikawa Y (1992). Conditions of energy and incident angle of primary beam for observation of insulator's surface by SEM. J. Electron Microsc. **41**: 65-69.

Lee KL, Schaefer C, Kern DP (1991). Surface grid technique for non-contact electron beam testing of very large scale integrated substrate. J. Vac. Sci. Technol (B) **9**: 1993 - 2005.

Le Gressus C, Vigouroux JP, Duraud JP, Boiziau C, Geller J (1984). Charge neutralization on insulators by electron bombardment. Scanning Electron Microsc. 1984; **I**: 41-48.

Niedrig H (1982). Electron backscattering from thin films. J. Appl. Phys. **53**: R15 - R49.

Nye P, Dinnis AR (1985). Extraction field and oxide charging in voltage contrast system. Scanning, **1**: 117 - 124

Salehi M, Flinn EA (1980). An experimental assessment of proposed universal yield curves for secondary electron emission. J. Phys. D.: Appl. Phys. **13**: 281 - 289.

Seggern H von (1985). Charging dynamics of dielectrics irradiated by low energy electrons. IEEE Trans. Nucl. Sci. **32 (4)**: 1503 - 1511.

Seiler H (1983). Secondary electron emission in the scanning electron microscope. J. Appl. Phys. **54**: R1 - R18.

Shaffner TJ, Hearle JWS. (1976). Recent advances in understanding specimen charging. Scanning Electron Microsc. 1976; **I**: 61 -70.

Silvester PP, Ferrari RL (1983). Finite Element for Electrical Engineer. Cambridge University Press, Cambridge: chapter **1**.

Sugiyama N, Ikeda S, Uchikawa Y (1986). Low voltage SEM inspection of micro-electronic devices. J. Electron Microsc. **35(1)**: 9-18.

Vaughan JRM (1989). A new formula for secondary emission yield. IEEE Trans. Electron Devices **36**: 1963 - 1967.

Wells OC (1974). Scanning Electron Microscopy. McGrow-Hill Book Company, New York: chapter **3**.

Wells OC (1975). Measurements of low-loss electron emission from amorphous targets. Scanning Electron Microsc. 1975; **I**: 43- 50.

Werner HW, Warmoltz N (1984). Beam techniques for the analysis of poorly conducting materials. J. Vac. Sci. Technol. (A) **2**: 726 - 731.

Discussion with Reviewers

LJ Balk: As far as I understood, you have not taken into account changes in energy of 2Es due to charging? Or at least it becomes not clear enough in section 7.

Authors: Charging affects the energy of 2Es indirectly through the electrostatic field and the velocity of 2Es. These have been taken into account in the program.

LJ Balk: Could you comment on the physical meaning of the cut-off energy E_0?

Authors: The cut-off energy E_0 is the critical energy below which no secondary electrons can be emitted. Secondary electrons are host electrons liberated by the incident electrons during inelastic collisions such as shell electron excitation, valence electron excitation, conduction electron excitation and plasma excitation. The cross-sections of these inelastic scattering processes increase with decreasing incident energy but drop sharply to almost zero after reaching a maximum. For most materials the cut-off is around 10 eV (Ho et al. 1991). Furthermore, the liberated electrons need to overcome the surface potential barrier to get to the surface.

LJ Balk: How critically is your calculation affected by the physically given boundary conditions such as dimensions of the specimen chamber, device holder, device itself, and last but not least, the dimensions of the insulating parts within a device?

Authors: The special structure presented in this paper has very large dimensions and the electric field within the central region is solely determined by the boundary conditions of the electrodes. As a result, the chamber wall, detector and specimen stage do not affect the calculations. In most practical situations, the detector, pole-piece, specimen stage and the chamber walls shape the electric field inside and outside the specimen and hence they require special attention.

The space in the SEM chamber is usually very large ($>$ 10 mm x 10 mm x 10 mm), whereas the size of the fine structures on the specimen surface could be smaller than 1 μm. The size of the finite element meshes inside and around the insulating parts of the specimen must be smaller than the size of the details on those parts so that the potential distribution inside and outside the insulators can be approximated accurately. If the entire free space in the chamber and the specimen itself are discretized into finite element meshes, then the large number of grid points will make calculations extremely slow or impossible. In most situations, it is convenient and desirable to construct some imaginary boundaries (representing the chamber walls, specimen stage and detector) which are much closer to the specimen. The voltage on these imaginary boundaries must be scaled proportionally. For any given set of imaginary

boundary conditions and domain discretization, the convergence of potential calculation using finite element method can be estimated easily. However, there is no way of estimating the closeness of this calculated potential to the actual potential. Electric potential calculation is the first computational step in the entire simulation sequence. Hence, any deviation of the calculated potential from the actual value affects the accuracy of the entire simulation. As a result, the choice of the imaginary boundaries and conditions are very critical. In our simulation, imaginary boundaries are chosen such that they are as far as possible from the specimen; but under the constraint that the total number of mesh points should not exceed 10,000.

Y Uchikawa: Since accuracy of numerical simulations always depends upon selection of parameters for discretization, one has to vary those parameters to find out whether or not the selections do affect the simulation results within the permissible limit of errors. Have you examined the accuracy of simulation that way?

F Hasselbach: Is a spatial tolerance factor ε_r as small as 0.1 um (Table I) necessary in order to get the theoretical (dotted and dashed lines) results of Fig 10. What happens when this constraint is relaxed considerably?

Authors: Vigorous efforts were made to check and improve the accuracy of simulations. In fact, the theoretical results shown in Fig. 10 are the best results (closest to experiment) obtained using the set of optimum parameters listed in Table I. For this particular simulation, the most critical parameter is the percentage factor R_c. Increasing R_c by a factor of 10 increases the simulation error by more than 10% (especially for negative extraction voltage). On the other hand reducing R_c by a factor of 10 gives a slight improvement in accuracy but increases the simulation time considerably. The physical dimension of the special set-up (Fig. 9) is very large, thus spatial tolerance factor (ε_r) as large as 10 μm can be used without significant increase in error. However, in simulation involving very small structures (such as integrated circuits), ε_r smaller than 0.1 μm is needed.

Our experience has shown that the accuracy of simulations involving small structures (such as integrated circuits) is very dependent on the choice of simulation parameters (energy and angular discretization, R_c, ε_r, ε_v and Δt). Considerable effort is required when choosing the optimum set of parameters. An improved version of the simulation program has been developed to overcome this problem.

In the improved program, the primary electrons (PEs) in a specific exposure time T_{EX} are represented by N (say 10000) super-electrons, each having energy E_{PE} and charge Q_n. When a super-electron impinges on a solid, two random numbers are cast to determine the number of SEs and BEs emitted. These random numbers are weighted by the yield curve of that particular solid material. For each emitted electron, a pair of random numbers is cast to determine its emission energy and direction. These two random numbers are weighted by the energy and angular distribution specific to that material for the given incident energy and angle. The charge of each emitted super-electron is equal to the charge of the incident super-electron. In this way, the accuracy of simulation is only determined by the choice of N and Δt. Furthermore, the population of traveling super-particles is much lower.

Only the super-particle generation section is modified; all other computational steps are identical to those presented in this paper.

AR Dinnis: Can you use your computer model to produce algorithms to correct readings obtained with commonly used detector systems in the presence of specimen charging?

Authors: Specimen charging in the SEM is a very local and dynamic phenomenon which depends on many parameters such as specimen material composition, surface roughness and topology, detector configuration and bias voltage, and beam current and energy. All these parameters must be correctly represented in the simulation model to give a realistic result that can be used to correct measurement errors due to specimen charging. Right now, only specimens with well defined material composition and surface topologies (such as integrated circuits) can be accurately modelled. We believe this program can produce algorithms to correct measurement errors due to specimen charging. The fields of applications are in e-beam testing of ICs and critical dimension measurement.

LJ Balk: What do you believe a 3D-calculation will realistically achieve? Is an extension to it sensible in a good effort/performance relation?

Authors: A 3-D system can extend the application of this program to (a) investigation of specimen charging in the presence of non-uniform magnetic fields, (b) evaluation of beam spot degradation (defocusing and astigmatism) due to specimen charging, (c) evaluation of stored charge induced placement and alignment errors during electron-beam lithography and (d) produce algorithms to correct for stored charged induced measurement errors during voltage contrast measurements and critical dimension measurements. Extending a 2-D finite element model into a 3-D model requires considerable effort. An user interface is now a must for specifying the geometries of specimen, detector and chamber walls. It is also needed to display the three dimensional potential and vector fields, charge distributions and electron trajectories. Despite these factors, we believe it is worthwhile to develop a 3-D system.

Y Uchikawa: In our previous papers (Ikeda and Uchikawa, 1981), (Uchikawa and Ikeda, 1981), (Uchikawa and Ikeda, 1983), (Sugiyama et al., 1986), (Sugiyama et al., 1988) we pointed out that ferroelectric domain contrast observed on such materials as Triglycine sulfate and Barium titanate in the SEM take a similar course of contrast variations to those observed on passivated semiconductor devices. We also reported that such contrast variations can be explained as a phenomenon due to specimen charging (Kodama et al., 1989), (Kodama and Uchikawa, 1992), (Ishibashi et al., 1992). Do you think that your simulation scheme can provide

a comprehensive interpretation of phenomena related to specimen charging including such contrast variations ?

Y Uchikawa: You stated in Introduction that your paper presents a numerical model to simulate the dynamics of specimen charging, but you discussed only results of the final stationary state of specimen charging. It is known that specimen charging in the SEM is a very local and dynamic phenomenon, since the fine probe of primaries scans very fast over the specimen surface. Will you mention some of your results concerning the transitional states of local potential variations?

AR Dinnis: While good practical results are obtained with your special set-up, do you have any convincing results for devices having dimensions typical of real integrated circuits?

Authors: Our simulation program is only capable of simulating contrast variations due to the change of electric field outside the specimen. We have used this program to study the dynamics of capacitively coupled voltage contrast (CCVC) in a passivated 2-micron integrated circuit and are able to explain some anomalous contrast phenomenon (Ookubo et al., 1986), (Kodama et al., 1989) that could not be explained using the conventional CCVC theory (Görlich et al. 1986). Right now we are not able to simulate contrast variations (Ishibashi et al., 1992), (Sugiyama et al., 1988), (Kodama and Uchikawa, 1992) which apparently are due to charging mechanisms inside the specimen.

AR Dinnis: Can you give some recommendations on the design of spectrometer and lens systems which minimize disadvantageous specimen charging? For example, is the use of magnetic immersion lens, which ensures that very few electrons return to the specimen, likely to improve measurement accuracy?

Authors: Right now, our simulation program can only accept electric boundary conditions, hence we are not in the position to recommend the design of SE spectrometers using magnetic lenses.

F Hasselbach: What are the hardware requirements for this model calculation? Were they done on a PC?

Authors: The program is written in FORTRAN-77 (FTN77/486, University of Salford). It can run on any i486 based IBM compatible PC equipped with 16 megabytes of memory.

Additional References

Görlich S, Hermann KD, Reiners W, Kubalek E (1986). Capacitive Coupling Voltage Contrast. Scanning Electron Microsc. 1986; **II**: 447-464.

Ho YC, Tan ZY, Wang XL, Chen JG (1991). A theory and monte carlo calculation on low energy electron scattering in solids. Scanning Microsc. Vol **5(4)**, 945 - 951.

Ikeda S, Uchikawa Y (1981). SEM imaging of ferroelectric domains. J. Electron Microsc. **29**, 209-217.

Kodama T, Ikeda S, Uchikawa Y (1989). A novel technique for voltage measurements of the passivation layer in SEM. J. Electron Microsc. Vol **38 (1)**, 6 - 15.

Ookubo K, Goto Y, Furukawa Y, Inagaki T (1986). Quantitative voltage waveform measurement technique for an IC internal electrode with a passivation film. Proc. **XIth** Int. Cong. on Electron Microsc., Kyoto, 631-632.

Sugiyama N, Ikeda S, Uchikawa Y (1988). SEM voltage contrast mechanism of passivated devices. Scanning Vol **10**, 3 - 8.

Uchikawa Y, Ikeda S (1981). Application of scanning electron microscopy (SEM) to analysis of surface domain structure of ferroelectrics. Scanning Electron Microsc. 81; **I:** 137-134.

Uchikawa Y, Ikeda S (1983). Inspection of micro devices over the passivated top-layer surface using the low voltage SEM. Jap. J. Appl. Phys. Vol **22(10)**, L645-L647.